A PATTERN JITTER FREE AFC SCHEME FOR MOBILE SATELLITE SYSTEMS

Shousei Yoshida
C&C Systems Research Laboratories, NEC Corporation
1-1, Miyazaki 4-chome, Miyamae-ku, Kawasaki 216, Japan
Phone +81-44-856-2122
Fax +81-44-856-2230

ABSTRACT

This paper describes a scheme for pattern jitter free automatic frequency control (AFC) with a wide frequency acquisition range. In this scheme, equalizing signals fed to the frequency discriminator allow pattern jitter free performance to be achieved for all roll-off factors. In order to define the acquisition range, frequency discrimination characteristics are analyzed on a newly derived frequency domain model. As a result, it is shown that a sufficiently wide acquisition range over a given system symbol rate can be achieved independent of symbol timing errors. Additionally, computer simulation demonstrates that frequency jitter performance improves in proportion to E_b/N_0 because pattern-dependent jitter is suppressed in the discriminator output. These results show significant promise for application to mobile satellite systems, which feature relatively low symbol rate transmission with an approximately 0.4-0.7 roll-off factor.

INTRODUCTION

In relatively low symbol rate transmission systems, such as mobile satellite systems, large carrier frequency offsets are induced by the frequency instability of a mobile terminal's oscillator and/or by the Doppler frequency shift. Such offsets may sometimes be as large as the symbol rate itself, and the automatic frequency control (AFC) loops [1], [2] commonly incorporated into satellite modems to eliminate frequency offsets prior to carrier phase recovery must have an acquisition range sufficient to handle the large offsets. Conventionally, such wide acquisition range is achieved by utilizing a continuous-wave (CW) pilot carrier. However, this results in poor frequency and power efficiency. Far better from this viewpoint would be the use of a modulated carrier.

When carrying out AFC with a band-limited MPSK modulated carrier, a single sample per a symbol period may be used for frequency discrimination. Then, the phase change for the modulated carrier over a full symbol contains the sum of the data symbol phase and the phase shift induced by frequency offsets. Hence, in order to be free from pattern jitter, the modulation must be removed by some nonlinear process such as an Mth-power operation for a signal point, i.e. an ISI free point to be sampled at $T_b/2$, where T_b is the symbol period. By this removal, however, the frequency offsets become M-fold, and the acquisition range is reduced to be within $\pm 1/2MT_b$. Furthermore, the nonlinear process produces a loss in carrier-to-noise ratio (C/N), which results in a degradation of frequency jitter performance of the AFC.

A scheme involving the measurement of a phase shift induced by frequency offsets between two samples in a symbol period has been proposed [3]. In this scheme, a root raised-cosine filter with 100 percent excess bandwidth is employed on the transmitter side to shape the pulse in such a way as to produce two inter-symbol interference (ISI) free points over half a symbol, and these two ISI free samples are used for detecting frequency errors to attain pattern jitter free performance. The usage of this filter, however, increases transmission frequency bandwidth. In band-efficient communication systems, such as mobile satellite systems, a pattern jitter free AFC scheme with a wide acquisition range, which can be applied to systems with smaller roll-off factors, is urgently needed. This paper proposes an advanced AFC scheme, in which equalizing signals fed to the frequency discriminator allow pattern jitter free performance to be achieved for all roll-off factors.

PATTERN JITTER FREE AFC SCHEME

With regard to frequency discrimination methods, cross-product frequency discrimination (CPFD) is widely used, which is especially well suited to digital implementation [1], [2]. CPFD operates to detect frequency errors by using two successive samples obtained from a CW carrier. Specifically, it calculates the sine of a phase shift induced by frequency offsets during a sample period. When carrying out AFC with a modulated carrier, in order to avoid an undesirable reduction in the acquisition range, frequency discrimination without explicit modulation removal is preferred. CPFD using two samples per a symbol period is

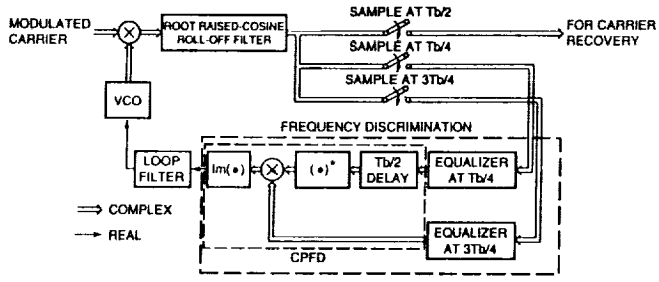

Figure 1. Proposed AFC scheme configuration.

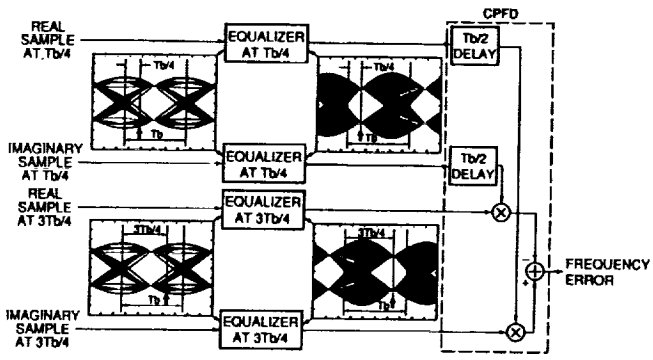

Figure 2. Frequency discrimination block diagram.

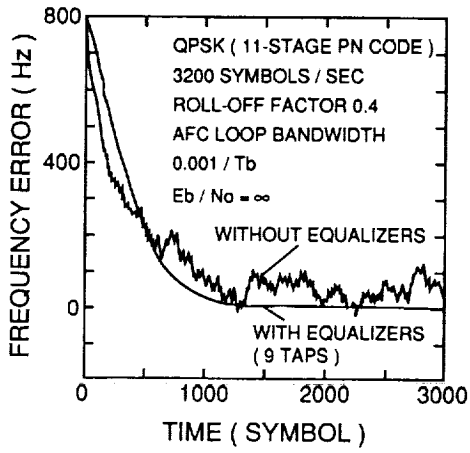

Figure 3. Frequency acquisition characteristics.

a possible approach. Root raised-cosine filtering with 100 percent excess bandwidth yields two ISI free points spaced $T_b/2$ apart and placed symmetrically with reference to the midpoint of the symbol period. Using these samples at $T_b/4$ and $3T_b/4$ for CPFD, pattern jitter free performance can be achieved. Without said filtering, however, these two ISI free points cannot be expected to be obtained, and the CPFD output will include pattern-dependent jitter. In order to combat such pattern jitter, the author has introduced two T_b-spaced equalizers to cancel out the ISI on the two samples in the symbol period, where $T_b/4$ and $3T_b/4$ has been chosen as the two sample timings to simplify the demodulator structure.

The proposed AFC scheme configuration is shown in Figure 1. Frequency offsets in an MPSK modulated carrier are first eliminated by a VCO output, and the result is passed through a root raised-cosine RX filter. The band-limited signal is sampled with optimum symbol timing at $T_b/2$ for later carrier phase recovery, and is subsequently sampled at $T_b/4$ and $3T_b/4$ for frequency discrimination. Since ISI naturally exists on these samples at $T_b/4$ and $3T_b/4$, equalizers work so as to cancel out the ISI before frequency discrimination (see Figure 2 for QPSK). The equalized samples at $T_b/4$ and $3T_b/4$ are fed to the frequency discriminator, where frequency errors are detected based on CPFD. The errors are averaged by a loop filter, and are utilized to control the VCO. Thus, pattern jitter free performance is achieved at the cost of a relatively small increase in complexity.

Frequency acquisition characteristics obtained by computer simulation are shown in Figure 3. The simulation was implemented for QPSK modulation at a 3200 symbols/sec rate. An 11-stage PN sequence was chosen as the modulation pattern. The roll-off factor for the RX filter was 0.4. The number of taps for the RX filter and for each equalizer was 9. The loop bandwidth for the AFC was set to be $0.001/T_b$. In the proposed scheme, pattern-dependent jitter is less than that occurring in the case without equalizers.

As has been mentioned above, although pattern-dependent jitter in the proposed scheme is definitely suppressed, it is difficult to understand intuitively the operation involved in detecting frequency errors in the acquisition stage. Specifically, it is of great interest to determine the possible influence exerted on the frequency discrimination characteristics by the two equalizers, which operate independently at $T_b/4$ and $3T_b/4$ sample timings. In an attempt to clarify the frequency error detecting operation, in the discussion which follows the author derives equalizer characteristics and attempts to define frequency discrimination characteristics analytically.

EQUALIZER CHARACTERISTICS

The equalizer spectrum characteristics can be derived from the spectrum characteristics of the channel filter. First, the impulse response $g(t)$ of a raised-cosine roll-off filter is sampled, where the sample period is T_b, and the sample timing difference from the midpoint of $g(t)$ is $\gamma T_b (-0.5 \leq \gamma < 0.5)$. The sampled signal $g_s(t)$ is expressed by

$$g_s(t) = g(t+\gamma T_b) \sum_{n=-\infty}^{\infty} \delta(t - nT_b)$$

$$= g(t+\gamma T_b) \frac{1}{T_b} \sum_{n=-\infty}^{\infty} e^{jn\omega_b t}$$

$$(\omega_b = 2\pi/T_b). \qquad (1)$$

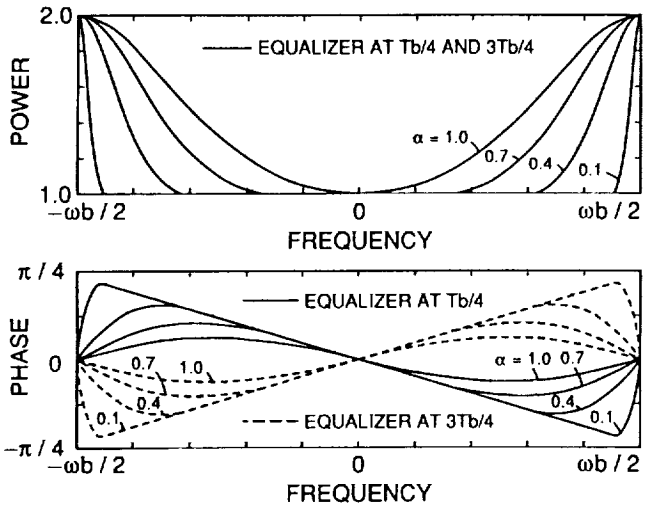

Figure 4. Equalizer spectra.

The Fourier transform $G_s(\omega)$ of $g_s(t)$ is written by

$$G_s(\omega) = \frac{1}{T_b} \sum_{n=-\infty}^{\infty} G(\omega - n\omega_b) e^{j(\omega - n\omega_b)\gamma T_b}. \quad (2)$$

Here, since $G(\omega)$ represents the raised-cosine roll-off spectrum, aliasing effects cause overlaps only to adjacent spectra.

$$\begin{aligned} G_s(\omega) &= \frac{1}{T_b}[G(\omega)e^{j\omega\gamma T_b} + G(\omega+\omega_b)e^{j(\omega+\omega_b)\gamma T_b} \\ &+ G(\omega-\omega_b)e^{j(\omega-\omega_b)\gamma T_b}] \\ &(-\omega_b/2 \le \omega < \omega_b/2). \end{aligned} \quad (3)$$

Substituting the raised-cosine roll-off spectrum $G(\omega)$ into (3), $G_s(\omega)$ may be rewritten as follows.

$$\begin{aligned} G_s(\omega) &= \frac{1}{T_b} e^{j\omega\gamma T_b} \quad (0 \le \omega < (1-\alpha)\omega_b/2) \\ &= \frac{1}{2T_b}\left\{1 - \sin\left[\frac{\pi(\omega - \omega_b/2)}{\alpha\omega_b}\right]\right\} e^{j\omega\gamma T_b} \\ &+ \frac{1}{2T_b}\left\{1 + \sin\left[\frac{\pi(\omega - \omega_b/2)}{\alpha\omega_b}\right]\right\} e^{j(\omega-\omega_b)\gamma T_b} \\ &((1-\alpha)\omega_b/2 \le \omega < \omega_b/2) \\ G_s(\omega) &= G_s^*(\omega) \quad (-\omega_b/2 \le \omega < 0) \end{aligned} \quad (4)$$

where α is the roll-off factor. The equalizer spectra are represented as $1/G_s(\omega)$. Figure 4 shows equalizer spectra at $T_b/4$ and $3T_b/4$, i.e. when $\gamma = 1/4$ and $-1/4$ in $1/G_s(\omega)$. Each equalizer works so as to zero-force both the amplitude distortion and the phase distortion of the folded spectrum $G_s(\omega)$ at around $\pm\omega_b/2$.

The impulse response $h_s(nT_b)$ of each equalizer, where n is an integer, is given by the inverse Fourier transform of $1/G_s(\omega)$.

$$h_s(nT_b) = \frac{1}{2\pi}\int_{-\omega_b/2}^{\omega_b/2} \frac{e^{j\omega nT_b}}{G_s(\omega)} d\omega. \quad (5)$$

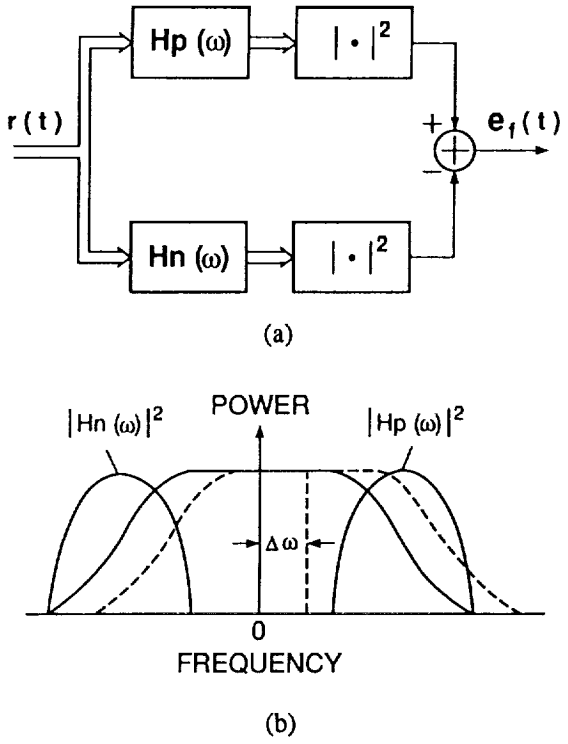

Figure 5. Differential power measurement frequency discrimination. (a) Block diagram. (b) Discrimination principle.

FREQUENCY DISCRIMINATION CHARACTERISTICS

In this section, in order to define the acquisition range for the proposed scheme, a new discrimination model is derived in the frequency domain, and it is used to analyze frequency discrimination characteristics.

Frequency Discrimination Model

It has previously shown that CPFD may be considered as equivalent to differential power measurement frequency discrimination (DPMFD) [4]. A DPMFD block diagram is given in Figure 5(a), and the discrimination principle is illustrated in Figure 5(b). In DPMFD, differential amounts of output power from two filters located respectively in positive and negative frequency bands are calculated as frequency errors. For CPFD which operates at a double symbol rate of $2/T_b$, the positive/negative filter spectra $H_p(\omega)$ and $H_n(\omega)$ may be expressed as follows.

$$\begin{aligned} H_p(\omega) &= \frac{1}{2}\left[e^{-j\omega T_b/4} - je^{j\omega T_b/4}\right] \\ H_n(\omega) &= \frac{1}{2}\left[e^{-j\omega T_b/4} + je^{j\omega T_b/4}\right]. \end{aligned} \quad (6)$$

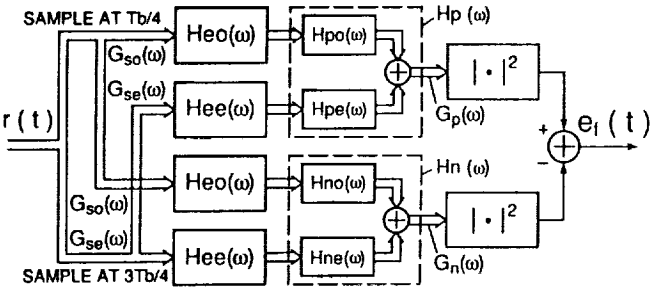

Figure 6. Frequency discrimination model.

In the proposed scheme, a sampled signal at $T_b/4$ and a sampled signal at $3T_b/4$ are fed to different T_b-spaced equalizers, which separately remove ISI at $T_b/4$ and $3T_b/4$. The results are input to the positive/negative filters in DPMFD. Here, since the positive/negative filters alternately receive the equalized signals at $T_b/4$ and $3T_b/4$, these filters are divided into two parts, i.e. one part for receiving an equalized signal at $T_b/4$ and another part for receiving an equalized signal at $3T_b/4$, and the two outputs are combined. Impulse responses $h_p(t)$ and $h_n(t)$ of the positive/negative filters are expressed by using impulse responses $h_{po}(t)$ and $h_{no}(t)$ at $T_b/4$, and impulse responses $h_{pe}(t)$ and $h_{ne}(t)$ at $3T_b/4$ as follows.

$$\begin{aligned} h_p(t) &= h_{po}(t + T_b/4) + h_{pe}(t - T_b/4) \\ h_n(t) &= h_{no}(t + T_b/4) + h_{ne}(t - T_b/4) \end{aligned} \quad (7)$$

where $h_{po}(t)$,$h_{pe}(t)$,$h_{no}(t)$ and $h_{ne}(t)$ are

$$\begin{aligned} h_{po}(t) &= -j\delta(t)/2 \quad h_{pe}(t) = \delta(t)/2 \\ h_{no}(t) &= j\delta(t)/2 \quad h_{ne}(t) = \delta(t)/2. \end{aligned} \quad (8)$$

The frequency discrimination model is shown in Figure 6. The positive/negative filter output spectra $G_p(\omega)$ and $G_n(\omega)$ are calculated by the following equations.

$$\begin{aligned} G_p(\omega) &= G_{so}(\omega)H_{eo}(\omega)H_{po}(\omega) + G_{se}(\omega)H_{ee}(\omega)H_{pe}(\omega) \\ G_n(\omega) &= G_{so}(\omega)H_{eo}(\omega)H_{no}(\omega) + G_{se}(\omega)H_{ee}(\omega)H_{ne}(\omega) \end{aligned} \quad (9)$$

where $G_{so}(\omega)$ and $G_{se}(\omega)$ are sampled signal spectra for $G(\omega)$ at $T_b/4$ and $3T_b/4$. Here, $G(\omega)$ is given by $G_t(\omega - \Delta\omega)H_r(\omega)$, where $G_t(\omega)$ and $H_r(\omega)$ are the TX signal spectrum and the RX filter spectrum respectively. Both have raised-cosine roll-off characteristics. $\Delta\omega$ values are frequency offsets. Furthermore, $H_{po}(\omega)$, $H_{pe}(\omega)$, $H_{no}(\omega)$ and $H_{ne}(\omega)$ are Fourier transforms of $h_{po}(t)$,$h_{pe}(t)$,$h_{no}(t)$ and $h_{ne}(t)$.

$$\begin{aligned} H_{po}(\omega) &= -j/2 \quad H_{pe}(\omega) = 1/2 \\ H_{no}(\omega) &= j/2 \quad H_{ne}(\omega) = 1/2. \end{aligned} \quad (10)$$

The $G_p(\omega)$ and $G_n(\omega)$ spectra for some $\Delta\omega$ values are computed as depicted in Figure 7.

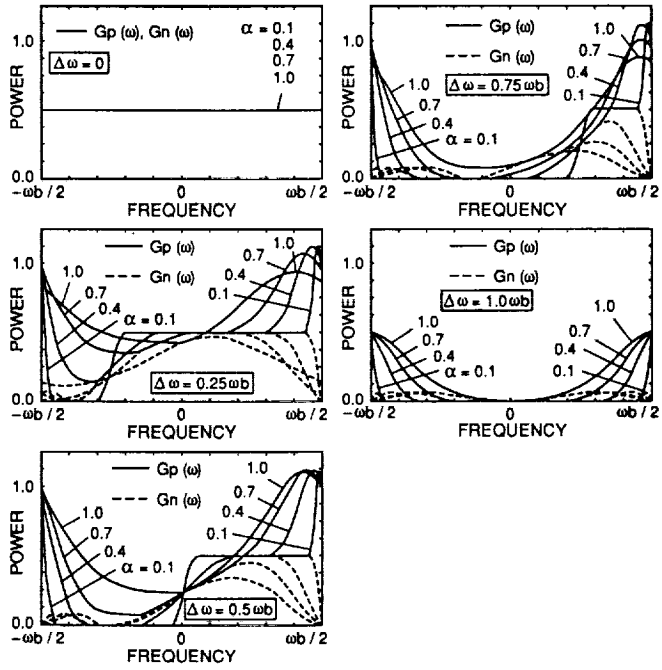

Figure 7. Positive/negative filter output spectra.

Frequency Discrimination Characteristics

Frequency errors are defined as the power difference between $G_p(\omega)$ and $G_n(\omega)$, i.e.

$$e_f = \int_{-\omega_b/2}^{\omega_b/2} |\, G_p(\omega) \,|^2 \, d\omega - \int_{-\omega_b/2}^{\omega_b/2} |\, G_n(\omega) \,|^2 \, d\omega. \quad (11)$$

Figure 8 shows frequency discrimination characteristics calculated using (11). It may be seen that a sufficiently wide acquisition range over a given system symbol rate can be achieved, and that the discrimination curves are dependent on roll-off factors. As the roll-off factor approximates 0.0, frequency error becomes smaller, gradually decreasing to zero. This is because the frequency range in which spectrum characteristics for $G_p(\omega)$ differ from those for $G_n(\omega)$ is reduced as the roll-off factor decreases (see Figure 7).

Frequency discrimination characteristics of the scheme using a CW carrier are shown together in Figure 8. The discrimination curves are represented as the product of sine function and root raised-cosine roll-off characteristics. Figure 8 also shows that the detection sensitivity, i.e. a differential coefficient at 0 Hz $\Delta\omega$ in the discrimination characteristics, of the proposed scheme is approximately half of that of the scheme using a CW carrier.

Frequency Discrimination Characteristics with Symbol Timing Errors

When the proposed scheme is implemented into mobile satellite modems, the symbol timing recovery influence in frequency acquisition should be discussed. For arbitrary

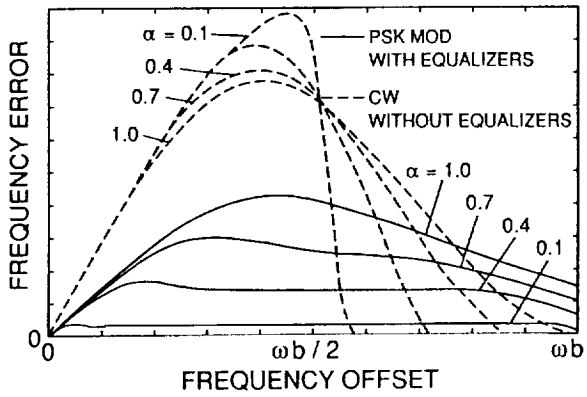

Figure 8. Frequency discrimination characteristics.

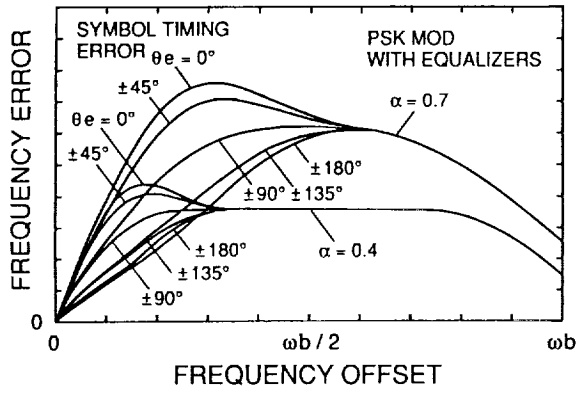

Figure 9. Frequency discrimination characteristics with symbol timing errors.

symbol timing errors $\theta_e(-180° \leq \theta_e \leq 180°)$, $G_{se}(\omega)$ and $G_{se}(\omega)$ represent sampled signal spectra for $G(\omega)$ at $(1/4-\theta_e/360°)T_b$ and $(3/4-\theta_e/360°)T_b$. Figure 9 shows frequency discrimination characteristics with symbol timing errors. Although the discrimination curves are dependent on symbol timing errors within a $\Delta\omega$ value of around $\omega_b/2$, the errors are still obtained with a wide frequency range. At more than $\Delta\omega$ value of $\omega_b/2$, the curves are made free from symbol timing errors. This is because there exist overlaps no longer in the folded spectra for the sampled signals at $(1/4-\theta_e/360°)T_b$ and $(3/4-\theta_e/360°)T_b$. In the proposed scheme, even if symbol timing is not recovered, frequency acquisition can be achieved with a wide acquisition range. After the symbol timing acquisition, pattern jitter free performance is attained.

SIMULATION RESULTS

The author has carried out a computer simulation to evaluate the proposed scheme for frequency jitter performance in the presence of Gaussian noise and for residual pattern jitter performance.

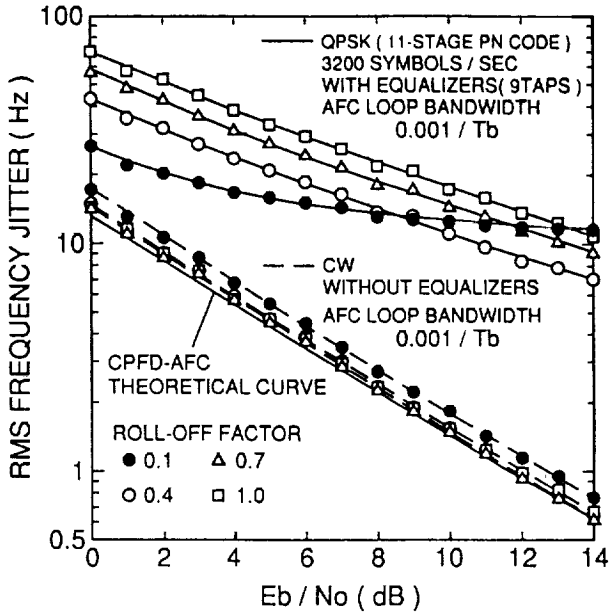

Figure 10. Frequency jitter performance in noise.

Frequency Jitter Performance in Noise

Figure 10 shows frequency jitter performance of the proposed scheme in the presence of noise. The simulation was implemented for QPSK modulation at a 3200 symbols/sec rate. An 11-stage PN sequence was chosen as the modulation pattern. The number of taps for the RX filter and for each equalizer was 9. The loop bandwidth for the AFC was set to be $0.001/T_b$. In the proposed scheme, frequency jitter performance improves in proportion to E_b/N_0, because pattern-dependent jitter is suppressed in the discriminator output. As the roll-off factor becomes smaller, the performance tends to be gradually degraded. In the case of too small a roll-off factor such as 0.1, residual pattern jitter due to imperfect equalization is dominant in the total frequency jitter performance.

The frequency jitter performance of the scheme using a CW carrier is shown together in Figure 10, in which the performance is independent of roll-off factors, and is consistent with the theoretical curve for CPFD-AFC [2]. The frequency jitter performance of the proposed scheme cannot be prevented from degrading as compared with that of the scheme using a CW carrier.

Residual Pattern Jitter Performance

Risidual pattern jitter performance of the proposed scheme was evaluated with regard to the number of taps for the equalizers, as shown in Figure 11. Although residual pattern jitter performance may be dependent on the modulation pattern, an 11-stage PN sequence was used as an example in the simulation. The loop bandwidth for the AFC was set to be $0.001/T_b$. Consequently, as the number

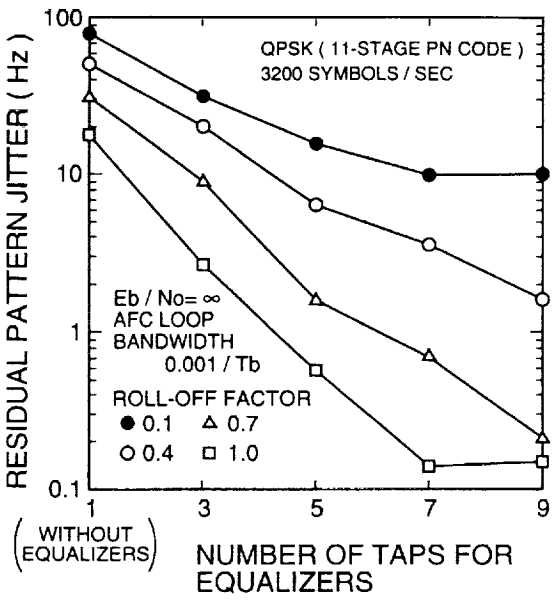

Figure 11. Residual pattern jitter performance.

of taps for the equalizers increases, residual pattern jitter performance improves. The improvement is greater for a larger roll-off factor, because impulse responses of the RX filter and of the equalizers with larger roll-off are shorter. By narrowing the AFC loop bandwidth, the performance may improve to some degree. This is, however, undesirable for suppressing pattern-dependent jitter, because the acquisition time increases. The number of taps for the equalizers should be designed to be as few as possible, if the pattern jitter is negligible in the total frequency jitter performance under operational E_b/N_0 conditions.

CONCLUSION

This paper has proposed a scheme for pattern jitter free AFC with a wide frequency acquisition range. In the proposed scheme, equalizing signals fed to the frequency discriminator allow pattern jitter free performance to be achieved for all roll-off factors. In order to define the acquisition range, frequency discrimination characteristics have been analyzed on a newly derived frequency domain model. As a result, it was shown that a sufficiently wide acquisition range over a given system symbol rate could be achieved independent of symbol timing errors.

Additionally, computer simulation has been carried out, which demonstrated that frequency jitter performance improved in proportion to E_b/N_0 owing to suppressing pattern-dependent jitter. These results showed significant promise for application to mobile satellite systems, which feature relatively low symbol rate transmission with an approximately 0.4-0.7 roll-off factor.

The author believes that applying the proposed concept to some other combination of the channel filters, e.g. a TX filter with root raised-cosine roll-off, a brick-wall RX filter for frequency discrimination [3] and another RX filter with root raised-cosine roll-off for data detection, were also possible. Those results were not discussed in this paper.

ACKNOWLEDGMENTS

The author wishes to thank Dr. Ushirokawa and Mr. Takeuchi and other members of C&C Systems Research Labs., NEC Corporation, for their helpful discussions.

REFERENCES

[1] C. R. Cahn, "Improving Frequency Acquisition of a Costas Loop," IEEE Trans. Commun., vol. COM-25, pp.1453-1459, Dec. 1977

[2] F. D. Natali, "AFC Tracking Algorithms," IEEE Trans. Commun., vol. COM-32, pp.935-947, Aug. 1984

[3] M. K. Simon, D. Divsalar, "Doppler-Corrected Differential Detection of MPSK," IEEE Trans. Commun., vol. COM-37, pp.99-109, Feb. 1989

[4] T. Alberty, V. Hespelt, "A New Pattern Jitter Free Frequency Error Detector," IEEE Trans. Commun., vol. COM-37, pp.159-163, Feb. 1989

Session 10
Modulation, Coding and Multiple Access

Session Chair—*Michael Miller,* University of South Australia, Australia
Session Organizer—*Robert Kwan,* Jet Propulsion Laboratory, U.S.A.

(continued)